Ubiquitinated PCNA Drives USP1 Synthetic Lethality in Cancer

Antoine Simoneau, Justin L. Engel, Madhavi Bandi, Katherine Lazarides, Shangtao Liu, Samuel R. Meier, Ashley H. Choi, Hongxiang Zhang, Binzhang Shen, Lauren Martires, Deepali Gotur, Truc V. Pham, Fang Li, Lina Gu, Shanzhong Gong, Minjie Zhang, Erik Wilker, Xuewen Pan, Douglas A. Whittington, Scott Throner, John P. Maxwell, Yingnan Chen, Yi Yu, Alan Huang, Jannik N. Andersen, and Tianshu Feng

ABSTRACT

CRISPR Cas9-based screening is a powerful approach for identifying and characterizing novel drug targets. Here, we elucidate the synthetic lethal mechanism of deubiquitinating enzyme USP1 in cancers with underlying DNA damage vulnerabilities, specifically *BRCA1/2* mutant tumors and a subset of *BRCA1/2* wild-type (WT) tumors. In sensitive cells, pharmacologic inhibition of USP1 leads to decreased DNA synthesis concomitant with S-phase–specific DNA damage. Genome-wide CRISPR-Cas9 screens identify *RAD18* and *UBE2K*, which promote PCNA mono- and polyubiquitination respectively, as mediators of *USP1* dependency. The accumulation of mono- and polyubiquitinated PCNA following USP1 inhibition is associated with reduced PCNA protein levels. Ectopic expression of WT or ubiquitin-dead K164R *PCNA* reverses USP1 inhibitor sensitivity. Our results show, for the first time, that *USP1* dependency hinges on the aberrant processing of mono- and polyubiquitinated PCNA. Moreover, this mechanism of *USP1* dependency extends beyond *BRCA1/2* mutant tumors to selected *BRCA1/2* WT cancer cell lines enriched in ovarian and lung lineages. We further show PARP and USP1 inhibition are strongly synergistic in *BRCA1/2* mutant tumors. We postulate *USP1* dependency unveils a previously uncharacterized vulnerability linked to posttranslational modifications of PCNA. Taken together, USP1 inhibition may represent a novel therapeutic strategy for *BRCA1/2* mutant tumors and a subset of *BRCA1/2* WT tumors.

Introduction

Synthetic lethality—a genetic interaction when the loss of two genes, but not either alone—leads to cell death and allows targeted therapies to selectively kill tumor cells while largely sparing normal cells. The approval of PARP inhibitors in *BRCA1/2* mutant cancer is the first clinical proof of concept for synthetic lethality (1). Given the success of PARP inhibitors, there has been considerable interest in the development of next-generation synthetic lethal cancer therapeutics. Recent advances in CRISPR-Cas9–based functional genomics, combined with improved knowledge of cancer genetics, are accelerating the targeting of novel genetic dependencies in cancer.

USP1 encodes a 785 amino acid cysteine protease belonging to the USP family of deubiquitinating enzymes (2). For optimized catalytic activity, USP1 forms a heterodimeric complex with UAF1 (2), a WD40 repeat-containing protein that also stimulates USP46 and USP12 (3). The USP1–UAF1 complex deubiquitinates several substrates involved in DNA damage response, including monoubiquitinated PCNA and FANCD2 (2, 4–6). USP1 plays a pivotal role in translesion synthesis (TLS) and template switching (TS) DNA damage tolerance processes that circumvent DNA lesions during or after DNA replication. The reversal of PCNA monoubiquitination by USP1 regulates TLS. Upon encountering damaged DNA, PCNA is monoubiquitinated at K164 by the Rad6-Rad18 ubiquitin ligase complex (7, 8). This facilitates the switch from high- to low-fidelity TLS polymerases, which lack proofreading activity and enable error-prone DNA lesion bypass (9–12). Monoubiquitinated PCNA may be further modified by K63-linked polyubiquitination (7, 13), which promotes error-free TS.

USP1 localizes to the replication fork to ensure processive DNA replication (14) and is critical for fork stability and protection in *BRCA1* mutant cells (14, 15). Although studies suggest TLS is critical for *USP1–BRCA1* synthetic lethality (15), the consequences of aberrant PCNA monoubiquitination remains unclear. In addition, USP1 has been implicated in the proliferation and survival of other cancers (16–18), suggesting alternate mechanisms of *USP1* dependency.

Using genetic and pharmacologic approaches, we describe the mechanism of *USP1* dependency in *BRCA1/2* mutant tumors and selected *BRCA1/2* WT lung and ovarian tumors. I-138, a literature compound structurally related to ML323 (19), displays improved potency and physiochemical properties suitable for *in vivo* studies. USP1 inhibition in sensitive cells results in aberrant accumulation of mono- and polyubiquitinated PCNA and reduced total PCNA levels. This is associated with decreased DNA synthesis, S-phase arrest, and DNA damage. Genome-wide CRISPR-Cas9 screens identify *RAD18* and *UBE2K* as key mediators of USP1 inhibitor sensitivity. In USP1 inhibitor-treated cells, *RAD18* knockout abrogates PCNA monoubiquitination, and *UBE2K* knockout reduces PCNA polyubiquitination. The loss of *RAD18* or *UBE2K* stabilizes PCNA protein levels and rescues USP1 inhibitor sensitivity. Similarly, *PCNA* overexpression rescues USP1 inhibitor sensitivity, indicating a central role for PCNA in USP1–BRCA1/2 synthetic lethality. Moreover, we show USP1 and PARP inhibitors are strongly synergistic in a BRCA1/2-dependent manner. In addition, a subset of HR-proficient ovarian and non–small

Tango Therapeutics, Boston, Massachusetts.

A. Simoneau, J.L. Engel, and M. Bandi contributed equally to this article.

Current address for J.L. Engel: UT Southwestern Medical Centre, Pathology, Dallas, Texas.

Corresponding Author: Tianshu Feng, Tango Therapeutics, 201 Brookline Avenue, Suite 901, Boston, MA 02215. E-mail: pfeng@tangotx.com

Mol Cancer Ther 2023;22:215–26

doi: 10.1158/1535-7163.MCT-22-0409

cell lung cancer cell lines are sensitive to USP1 inhibition. In both *BRCA1/2* mutant and WT tumors, *USP1* dependency converges on PCNA ubiquitination, suggestive of a novel DNA damage vulnerability that spans genetic and histologic backgrounds. Taken together, our results support USP1 as a promising oncology drug target.

Materials and Methods

Compounds

ML323 (HY-17543), olaparib (HY-10162), niraparib (HY-10619B), and gemcitabine (HY-17026) were purchased from MedChemExpress. Hydroxyurea (H8627) was purchased from Sigma-Aldrich. I-138 (2-(2-isopropylphenyl)-9-(4-(1-methyl-4-(trifluoromethyl)-1H-imidazol-2-yl)benzyl)-7,9-dihydro-8H-purin-8-one) was synthesized in a similar manner as described in US patent application US 2017/07145012 (20) and experimental details are described in Supplementary Materials and Methods.

Cell culture and cell-line engineering

Cell lines were purchased from vendors including Horizon Discovery, ATCC, JCRB, EECACC, RIKEN, and Takara Bio (Supplementary Table S1). All cell lines were cultured and maintained in 37°C incubators with 5% CO_2. Cell lines were confirmed by STR (Labcorp), routinely tested for mycoplasma (Lonza; MycoAlert Mycoplasma Detection Kit, LT07–418), and used up to passage 13. For CRISPR-Cas9 experiments, *Cas9*-expressing stable cells were generated. Lentivirus was generated by transfecting constructs and lentiviral packaging mix (Cellecta, CPCP-K2A) with Lipofectamine 3000 (Thermo Fisher Scientific, L3000015) in Lenti-X cells. After incubation with transfection reagents overnight, media was replaced with DMEM + 30% FBS. Media containing viruses was collected 48 hours after transfection and filtered with a 0.45-μm membrane. For infection, cells were incubated overnight in media containing 8 μg/mL polybrene (Sigma-Aldrich) and virus. Infected cells were recovered for 24 hours before selection with puromycin (Gibco, A1113802), blasticidin (Gibco, A1113903), or geneticin (Gibco, 10131035).

CRISPR-cas9 screening

Cas9-expressing cells were transduced with lentivirus containing CRISPR-Cas9 libraries (druggable genome or UMI) at multiplicity of infection of 0.3 to ensure an infection rate of one sgRNA per cell. For *BRCA1/2* target discovery screens, day 0 of the screen started at 72 hours after puromycin selection. For USP1 inhibitor screens in MDA-MB-436 and NCI-H1693, cells were divided into DMSO, 50 nmol/L I-138 (continuous treatment) and 200 nmol/L I-138 (5 days on, 5 days off) arms at 72 hours after infection. Cells were allowed to adhere overnight in puromycin-containing medium before drug treatment (day 0). Screens were performed for 14 days in 23132/87, A549, AU565, FADU, HCC1954, SNU-638, HGC-27, KP4, NUGC-4, SNU-5, MDA-MB-231, HCC38, and HCC70. For SUM149PT, NCI-H1693, and MDA-MB-436, screens were performed for 21 days. Cell lines were subcultured twice a week and a library coverage of >1,000 cells were maintained throughout. Cells were harvested by PBS wash followed by trypsinization for gDNA extraction. gDNA from cell pellets was isolated using the QIAamp Blood Maxi Kit (Qiagen, 51194) and genome-integrated sgRNA sequences were amplified by PCR using HotStart ReadyMix (Roche, KK2602). Samples preparations was done amplifying the sgRNA with primers forward: F: 5′- AATGATACGGCGACCACCGAGATCTACACTCTTTCCCTACACGACGCTCTTCCGATCTNNNNNNNNNNCTTGTGGAAAGGACGAAACACCG-3′, reverse: R: 5′-CAAGCAGAAGACGGCATACGAGATNNNNNNNNGTGACTGGAGTTCAGACGTGTGCTCTTCCGATCT-3′, final Kapa Pure Beads (Roche, KK8802) purified products were sequenced on Illumina NextSeq500 systems. Computational analyses are described in Supplementary Materials and Methods.

Cell viability assays

For CellTiter-glo viability assay, cells were seeded onto 96- or 384-well plates (Corning) and allowed to adhere overnight. Drugs were added using a Tecan Digital Dispenser D300e (Hewlett-Packard). After 7 to 10 days, CellTiter-glo 2.0 reagent (Promega, G9243) was added to plates following manufacturer's instructions, and plates were incubated for 15 minutes protected from light. Luminescence was measured using EnVision multimode plate reader (EnVision Manager software v1.13.3009.1409; Perkin-Elmer). Cell viability was normalized against wells treated with DMSO (100%) or 10 μmol/L MG132 (0%). Dose–response was visualized using GraphPad Prism 9 nonlinear regression curve-fitting model. Combination studies were analyzed using Combenefit v2.021 (21).

For clonogenic survival assay, cells were seeded in 6-well plates 24 hours before drug treatment. Media with fresh compound was replaced every 3 to 4 days. After incubation for 10 to 17 days, cells were washed with PBS prior to addition of 0.25% crystal violet in 20% methanol. After staining for 5 minutes, plates were washed with water then allowed to dry. Plates were scanned with the LI-COR Odyssey Clx equipped with Image Studio software v5.2.

Biochemistry assay

Recombinant USP1-UAF1 proteins were expressed using Bac-to-Bac Baculovirus expression system (Thermo Fisher Scientific, 10359016) and purified to homogeneity (Biortus). USP1 activity was measured at room temperature in assay buffer containing 50 mmol/L HEPES pH 7.0, 0.5 mmol/L EDTA, 100 mmol/L NaCl, 10 mmol/L TCEP, 1.5 μmol/L BSA, 0.005% Tween20. 0.2 nmol/L USP1-UAF1 was incubated with compounds at room temperature for 15 minutes. Unlabeled ubiquitin (RD system, U-100H-10M-06311321A) was added and incubated for 15 minutes. Finally, 0.2 μmol/L Ub-Rho (Ubiquitin-Rhodamine110-Gly; Ubiquigent, 60–0117-BUL) was added. The results were recorded on BMG PHERAstar FSX microplate reader in Kinetic mode (Ex480/Em540; Gain 500).

DNA fiber assay

DNA fiber assays were performed as described previously (22), except cells were treated with 500 nmol/L I-138 for 4, 24, or 48 hours before and during CldU/IdU labeling. Images were acquired with a Zeiss Axioimager M2 equipped with Zen software v2.3 and analyzed with Fiji software v1.53q (23). Samples were blinded during the protocol and de-blinded after analysis.

EdU staining and immunofluorescence

EdU staining, PCNA, and ub-PCNA immunofluorescence experiments were performed as described previously (24). PCNA and ub-PCNA antibodies were used at a 1:500 dilution. For γH2AX immunofluorescence and antibodies, see Supplementary Materials and Methods for details.

Flow cytometry

Cells were seeded 24 hours before treatment. Annexin V was stained using FITC Annexin V Apoptosis Detection Kit (BD Biosciences,

556547). Cells were trypsinized, washed twice with PBS, and resuspended in 100 μL of Annexin V binding buffer. Cells were incubated in the dark for 15 minutes after adding 5 μL of Annexin V-FITC and 5 μL of propidium iodide (PI). Next, 400 μL of Annexin V binding buffer was added, and cells were passed through a filter to remove clumps. For cell-cycle analysis, treated cells were trypsinized, washed twice with PBS, and fixed using ice-cold 70% ethanol. Cells were washed twice with PBS and resuspended in 500 μL of FxCycle PI/RNase staining solution (Invitrogen, F10797) and incubated at room temperature for 30 minutes. All flow cytometry experiments were performed on Agilent NovoCyte flow cytometer (Agilent) and analyzed using FlowJo v10.8.1 or Agilent NovoExpress v1.5.6.

Immunoblotting and MS

Protein lysate preparation, immunoblotting, and MS experiments were performed as described previously (25). Antibodies are summarized in Supplementary Table S2.

RT-qPCR

Cells were treated with RNA Cell Lysis Buffer (Boston Bioproducts, R-108) supplemented with 1:40 dilution of RNasin (VWR, PAN2611) and incubated for 5 minutes at room temperature. qRT-PCR reaction was prepared using TaqMan Fast Virus 1-Step Master Mix (Life Technologies, 4444436) according to manufacturer's protocol. For a final volume of 10 μL, 1 μL of template was added to the 384-well plate (Applied Biosystems, 4309849). A PrimeTime Std qPCR Assay was used to detect PCNA with a 6-FAM/ZEN/IBFQ 5′-3′ quencher (Integrated DNA Technologies, 326107661). Human RPLPO-VIC/MGB (Life Technologies, 4326314E) was used for normalization and was plexed with *PCNA* probe for all samples. Reaction was performed using QuantStudio 6 Flex.

Xenograft studies

Animal studies were performed in Pharmaron (China). Six- and 8-week-old female NOD SCID mice were supplied by AKYB (China) and maintained and handled under the approval of Institutional Animal Care and Use Committee (IACUC) of Pharmaron. After 7 days of acclimatization, 100-μL mixture containing 1:1 PBS and Matrigel with 10 million MDA-MB-436 cells were injected subcutaneously into the right flank of each animal. Once the tumors reached 150 to 200 mm^3 in size, animals were randomized to $N = 8$ groups. Mice were dosed by oral gavage once daily. Niraparib was administered at 15 and 10 mL/kg, in 0.5% w/v methylcellulose (Sigma-Aldrich, M0387). I-138 was administered at 50 mg/kg and 10 mL/kg, in 10% DMA (SAFC, ARK2190) + 50% solutol HS-15 (Sigma-Aldrich, 42966) + 40% capryol 90 (Gattefosse SAS, 3254BFE). Tumor volume was measured using a caliper and calculated as (length × width × width)/2.

Data availability statement

The data generated in this study are available within the article and its Supplementary files. High-throughput functional genomics data are available at the GEO repository, accession No. GSE214121.

Results

Identification of USP1 as a synthetic lethal target in *BRCA1/2* mutant tumors

To identify synthetic lethal targets in *BRCA1/2* mutant tumors, we performed CRISPR-Cas9 screens in 11 *BRCA1/2* WT and two *BRCA1* mutant cancer cell lines using a druggable genome library. Hits in *BRCA1* mutant cell lines were compared against those from WT cell lines using MAGeCK (**Fig. 1A**; Supplementary Table S1; ref. 26). We found known synthetic lethal targets including *PARP1* (27, 28), *POLQ* (29), *CHD1 L* (30), and *FANCD2* (31). *BRCA1* or *RAD51* depletion by CRISPR-Cas9 selectively targeted *BRCA1/2* WT but not mutant cells, consistent with homologous recombination deficiency due to *BRCA1/2* mutations. In addition, we identified *USP1* as a synthetic lethal target. We interrogated *USP1* dependency using publicly available CRISPR-Cas9 screening datasets (DepMap Public 22Q1; refs. 32, 33). Consistent with published literature (15), *USP1* depletion preferentially affected the proliferation of cell lines with biallelic *BRCA1* loss-of-function in projects Achilles and Score (**Fig. 1B**). Although the only *BRCA2* mutant cell line in this dataset, PEO1, was not sensitive to *USP1* depletion, presented but unpublished work from us and others have shown USP1 inhibitor activity in *BRCA2* mutant PDX models.

To evaluate USP1 as a potential drug target, we synthesized previously reported inhibitors of the USP1–UAF1 complex, ML323 and I-138 (**Fig. 1C**; refs. 19, 20). In an Ub-Rho cleavage assay, these compounds significantly inhibited USP1–UAF1 (**Fig. 1D**). We investigated the mode of USP1–UAF1 inhibition by I-138 using mutual exclusivity experiments. I-138 displayed synergistic binding with ubiquitin and mutual exclusive binding with ML323 (**Fig. 1E**; Supplementary Figs. S1A and S1B). Saturating concentrations of ubiquitin decreased its IC_{50}, whereas ML323 increased its IC_{50}. These results strongly suggest that I-138 binds to USP1–UAF1 at an allosteric pocket synergistically with ubiquitin, likely at the same site as ML323 (34). I-138 showed exquisite selectivity across a panel of 45 deubiquitinating enzymes (Ubiquigent DUB*profiler*; **Fig. 1F**). Fifty percent of inhibition of the closely related USP12–UAF1 and USP46–UAF1 complexes only occurred at 10 μmol/L compared with USP1-UAF1 IC_{50} of 4.1 nmol/L, reflecting a >2,000-fold selectivity.

Next, we assessed on-target activity of I-138 using *USP1* isogenic HAP-1 cells. *USP1* knockout HAP-1 cells exhibited persistent monoubiquitination of known substrates PCNA and FANCD2 (**Fig. 1G**). I-138 treatment increased PCNA and FANCD2 monoubiquitination in HAP-1 *USP1* WT but not knockout cells, indicative of an epistatic effect. In MDA-MB-436 cells, I-138 induced the monoubiquitination of FANCD2 and PCNA (**Fig. 1H**). Furthermore, I-138 ablated USP1 autocleavage in cells (6), consistent with inhibition of USP1 enzymatic activity (**Fig. 1G** and **H**). To assess I-138 pharmacodynamic modulation using an orthogonal assay, we measured PCNA monoubiquitination by immunofluorescence. The accumulation of monoubiquitinated PCNA was detectable within 4 hours of drug exposure in cells, consistent with USP1 inhibition (**Fig. 1I**; Supplementary Fig. S1C). These data show that I-138 is a potent and selective USP1–UAF1 inhibitor (abbreviated as USP1 inhibitor) displaying cellular target engagement.

USP1 inhibition causes replication stress and viability loss in *BRCA1/2* mutant cells

To validate USP1 as a synthetic lethal target, we determined the effect of USP1 inhibition on the viability of *BRCA1/2* WT and mutant cells (**Fig. 2A** and **B**; Supplementary Figs. S2A and S2B). USP1 inhibition selectively reduced the viability of the *BRCA1* mutant breast cancer cell line MDA-MB-436, but not the WT breast cancer cell line HCC1954 (**Fig. 2A**). Similarly, USP1 inhibition caused viability loss in *BRCA1* mutant ovarian cancer cell line UWB1.289 (**Fig. 2B**). *BRCA1* re-expression in UWB1.289 rescued USP1 inhibitor sensitivity, consistent with a synthetic lethal interaction. Next, we evaluated the effect of USP1 inhibition in a panel of *BRCA1/2* WT and mutant cell lines (Supplementary Figs. S2A and S2B). USP1 inhibition led to viability

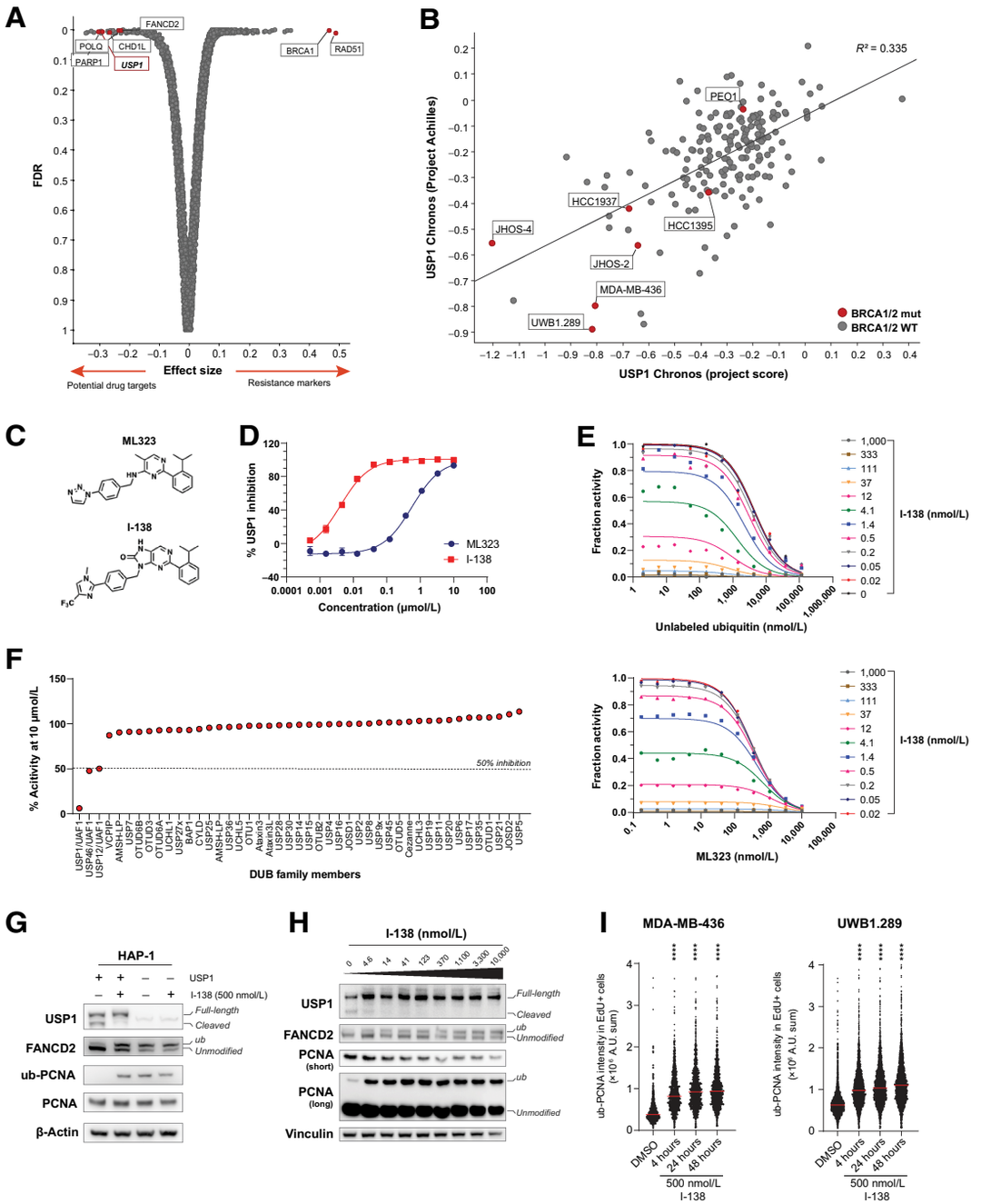

Figure 1.

USP1 is a synthetic lethal target in *BRCA1/2* mutant tumors amenable to small molecule inhibition. **A,** Volcano plot showing MAGeCK analysis comparing CRISPR-Cas9 screens performed in 11 *BRCA1/2* WT versus two *BRCA1* mutant breast cancer cell lines. Genes on the left are preferentially depleted in the *BRCA1* mutant compared with WT cells, whereas genes on the right are preferentially depleted in *BRCA1/2* WT compared to mutant cells. **B,** *USP1* Chronos from CRISPR screen datasets in projects Achilles and Score (DepMap Public, Q122). **C,** Chemical structures of literature USP1-UAF1 inhibitors ML323 (top) and I-138 (bottom). **D,** Activity of I-138 (IC_{50} 4.1 nmol/L) and ML323 (IC_{50} 569 nmol/L) in an USP1-UAF1 ubiquitin-Rhodamine 110 cleavage assay. **E,** Top panel shows mutual exclusive test of I-138 and ubiquitin (top). The result was fitted to modified Yontenani and Theorell equation to obtain $K_{I\text{-}138}$ (5.4 nmol/L), $K_{Ubiquitin}$ (4.5 μmol/L), and α (0.16). Bottom panel shows mutual exclusive test of I-138 and ML323. The result was fitted to modified Yontenani and Theorell equation to obtain $K_{I\text{-}138}$ (3.2 nmol/L), $K_{Ubiquitin}$ (341 nmol/L), and α (12.1). **F,** I-138 profiling in a biochemical assay panel of 45 deubiquitinating enzymes at the fixed concentration of 10 μmol/L (Ubiquigent DUBprofiler). **G,** Immunoblotting analysis of HAP-1 *USP1* WT and knockout cells treated with DMSO mock or 500 nmol/L I-138 for 4 hours. **H,** Immunblotting analysis of MDA-MB-436 whole cell lysates treated in indicated concentrations of I-138 for 24 hours. DMSO concentration was normalized across all conditions. **I,** Quantitation of ub-PCNA intensity in MDA-MB-436 cells treated with I-138 at indicated concentrations and time points and stained with immunofluorescence. Statistical significance was evaluated by ANOVA followed by Dunett *post hoc* test comparing treatment conditions against DMSO control (****, $P < 0.0001$).

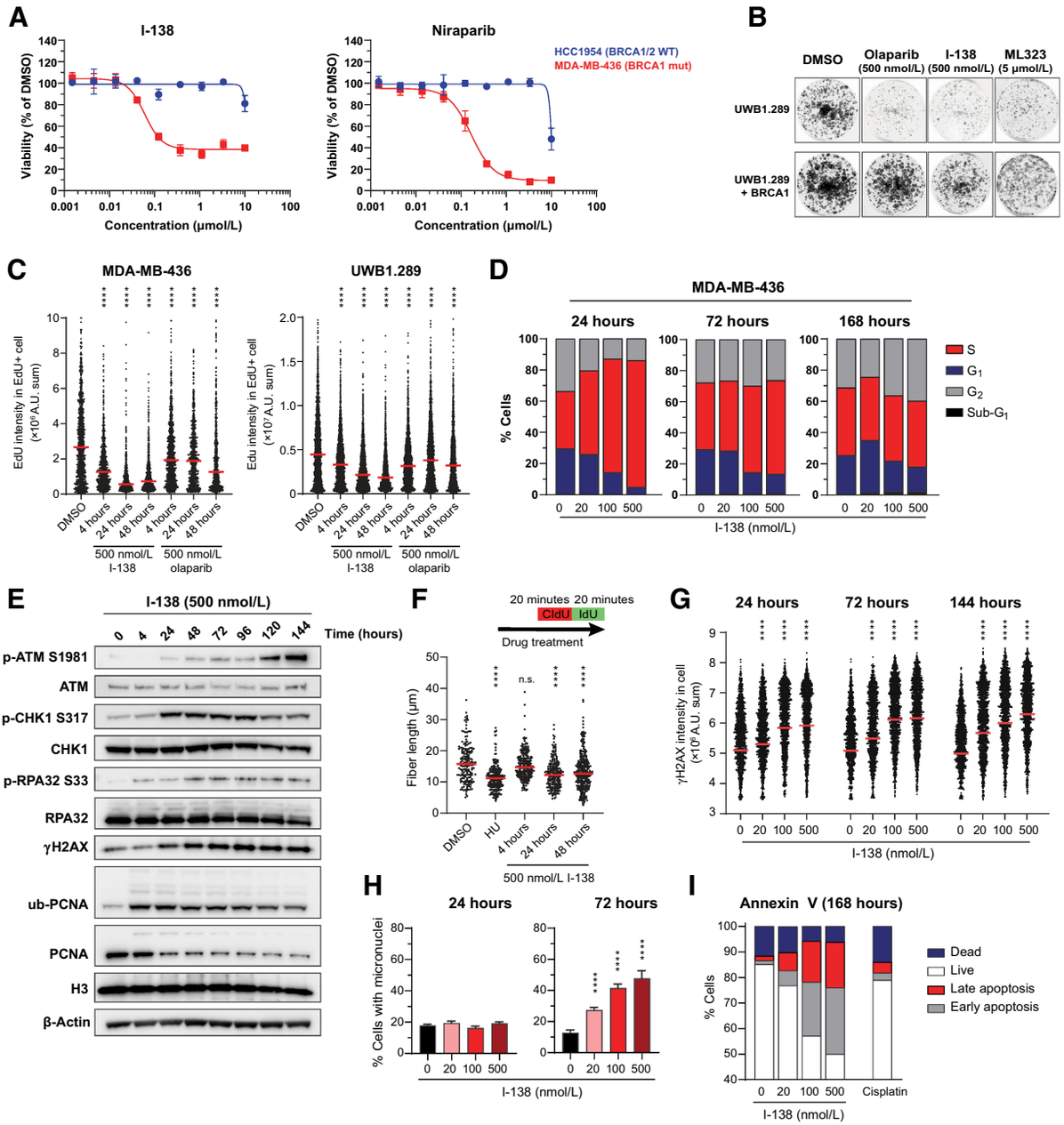

Figure 2.

USP1 inhibition causes loss of viability and replication stress in *BRCA1/2* mutant cells. **A,** Dose–response curves of MDA-MB-436 and HCC1954 cells treated with I-138 (left) or niraparib (right). Cells were seeded in 96-well plates and incubated in drug under normalized DMSO conditions for 10 days. Cell viability was estimated using CellTiter-Glo. **B,** Clonogenic assays performed using isogenic UWB1.289 cells with and without *BRCA1* re-expression. Cells were treated with indicated compounds for 14 days with media change every 3 to 4 days and visualized using crystal violet. **C,** Quantitation of EdU intensity in MDA-MB-436 (left) and UWB1.289 (right) cells pulsed-labelled with EdU after mock or compound treatment for indicated durations. Statistical significance was evaluated by ANOVA followed by Dunett *post hoc* test, comparing treatment conditions against DMSO control (****, $P < 0.0001$). **D,** Flow cytometry-based cell-cycle analysis of MDA-MB-436 cells treated with USP1 inhibitor and stained with propidium iodide. **E,** Immunoblotting analysis of MDA-MB-436 whole cell lysates, collected after treatment with 500 nmol/L I-138 at indicated time points under normalized DMSO conditions. **F,** Replication fork speed of MDA-MB-436 cells treated with DMSO, hydroxyurea, or I-138, measured with DNA fiber assay following the labeling schematic as shown. Statistical significance was evaluated by ANOVA followed by Dunett *post hoc* test, comparing treatment conditions against DMSO control (****, $P < 0.0001$; n.s., not significant). **G,** Quantitation of γ2HAX intensity in MDA-MB-436 cells stained with immunofluorescence treated with I-138 across multiple time points. Statistical significance was evaluated by ANOVA followed by Dunett *post hoc* test, comparing treatment conditions against DMSO control (****, $P < 0.0001$). **H,** Quantitation of micronuclei formation in MDA-MB-436 cells based on fluorescence imaging, where the percentage of cells with micronuclei were calculated from cells imaged in an entire well of a 96-well plate. Results are shown as mean ± SD, $N = 3$. Statistical significance was evaluated by ANOVA followed by Dunett *post hoc* test, comparing treatment conditions against DMSO control (****, $P < 0.0001$). **I,** Cell death in MDA-MB-436 treated with DMSO mock or USP1 inhibitor for 168 hours, measured using a flow cytometry–based Annexin V assay.

loss in *BRCA1* mutant cell lines JHOS-4, MDA-MB-436, and UWB1.289 (Supplementary Fig. S2A). *BRCA1* mutant cell lines relatively insensitive to olaparib, including SUM149PT, COV362, and JHOS-2, were unresponsive to USP1 inhibition. USP1 inhibitor treatment did not affect the viability of *BRCA1/2* WT breast and ovarian cancer cell lines, or the normal mammary epithelial cell line MCF10A (Supplementary Fig. S2B). I-138 activity correlated well with *USP1* Chronos (DepMap Public 22Q1), which supports its on-target profile as an USP1 inhibitor (Supplementary Fig. S2C).

Next, we interrogated the effect of USP1 inhibition on DNA replication and cell cycle. Asynchronous MDA-MB-436 and UWB1.289 cells were pulse labelled with EdU after 4, 24, and 48 hours of USP1 or PARP inhibitor treatment. USP1 inhibition significantly reduced the rate of DNA synthesis within 4 hours, whereas similar effects were only observed for olaparib at 48 hours (**Fig. 2C**). Concomitant with reduced DNA synthesis, USP1 inhibitor-treated cells transiently accumulated in S-phase at 24 hours, followed by gradual progression through the cell cycle (**Fig. 2D**). To determine whether USP1 inhibition affects replication speed, MDA-MB-436 cells were pulse labeled sequentially with chlorodeoxyuridine (CldU) and iododeoxyuridine (IdU) thymidine analogs. DNA fibers labeled with both nucleotide analogs were measured as a surrogate for replication fork speed. Consistent with published literature (14), USP1 inhibition significantly decreased the speed of replication elongation (**Fig. 2F**).

We asked whether USP1 inhibition in sensitive cells induces DNA damage. ATR signaling cascade was visualized by immunoblotting MDA-MB-436 cells treated with USP1 inhibitor over 6 days. RPA S33 and Chk1 S317 phosphorylation occurred at 4 and 24 hours after USP1 inhibition, consistent with replication stress and ATR activation (**Fig. 2E**). After 24 hours, we observed persistent γH2AX S139 phosphorylation and foci formation (**Fig. 2E** and **G**). ATM S1981 phosphorylation occurred at 24 hours and became more pronounced at 120 and 144 hours posttreatment, indicating increased DNA damage (**Fig. 2E**). Prolonged USP1 inhibition resulted in mitotic defects and cell death in MDA-MB-436 cells, evidenced by increased micronuclei formation and Annexin V staining (**Fig. 2H** and **I**). Taken together, our results suggest USP1 inhibition elicits DNA damage and replication stress, thereby causing cell-cycle arrest followed by death in *BRCA1/2* mutant cells.

PCNA ubiquitination and protein loss mediate *USP1* dependency

To elucidate the mechanism of *USP1* dependency, we performed genome-wide dropout CRISPR-Cas9 screens to identify genes that rescue USP1 inhibitor sensitivity. The CRISPR-Cas9 unique molecular identifier (UMI) library links individual single-guide RNA (sgRNAs) to UMIs (**Fig. 3A**), which accounts for outlier clones and heterogeneous editing efficiency (35). MDA-MB-436 cells were treated with DMSO, 50 nmol/L (IC_{50}; continuously), or 200 nmol/L (IC_{80}; 5 days on 5 days off) of USP1 inhibitor following viral transduction (**Fig. 3A**). The results were analyzed using two computational approaches. The first approach integrated UMI counts with conventional MAGeCK pipeline (26). In the second approach, the probability of UMI count depletion or enrichment among the total number of UMIs for each sgRNA is modeled by a β-binomial distribution. We termed this novel nonparametric Bayesian method UMI Bayesian beta-binomial (UMIBB).

CRISPR-Cas9 UMI screens performed in the presence of 50 or 200 nmol/L compound were compared against that of DMSO (Supplementary Tables S2 and S3). Analyses incorporating UMIs yielded significantly less hits than conventional MAGeCK, likely due to elimination of low-confidence positives (**Fig. 3B**; Supplementary Fig. S3A; Supplementary Table S4). One example is the supposedly rescuing gene *RPTOR*, where the increased sgRNA counts were dominated by a few clones in contrast to high-confidence hits (Supplementary Figs. S3B and S3D). The three highest scoring genes from the CRISPR-UMI analyses were *RAD18*, *UBE2K*, and *UBE2A*. CRISPR-Cas9 guides targeting these genes were consistently enriched in inhibitor-treated cells relative to DMSO control, across multiple sgRNA sequences and clonal populations (**Fig. 3C**; Supplementary Figs. S3B–S3D).

To validate screen hits, we generated *RAD18* and *UBE2K* knockout cells in MDA-MB-436 background. RAD18 and UBE2A form the ubiquitin ligase complex that monoubiquitinates PCNA at K164 (7, 36). UBE2K is an E2 ubiquitin-conjugating enzyme that synthesizes K48-linked polyubiquitin chains (37). The loss of *RAD18* or *UBE2K*, confirmed by immunoblotting, rescued USP1 inhibitor sensitivity (**Fig. 3D** and **E**). Because RAD18 is directly involved in PCNA monoubiquitination (7, 36), we assessed the consequence of *RAD18* and *UBE2K* depletion on PCNA posttranslational modifications. Immunoblotting revealed that USP1 inhibitor increased the levels of mono- and polyubiquitinated PCNA in MDA-MB-436 (**Fig. 3E**; Supplementary Fig. S3E). As expected, *RAD18* knockout significantly reduced PCNA monoubiquitination upon USP1 inhibition (**Fig. 3E**; Supplementary Fig. S3E). Because PCNA monoubiquitination is a prerequisite for polyubiquitin chain elongation, *RAD18* knockout also abrogated PCNA polyubiquitination. In comparison, *UBE2K* knockout exclusively affected the levels of polyubiquitinated PCNA in drug-treated MDA-MB-436 cells. These suggest that UBE2K has a previously unreported role in promoting polyubiquitination in the context of persistent PCNA monoubiquitination.

We noted that USP1 inhibition reduced the levels of unmodified PCNA, which was restored upon *RAD18* or *UBE2K* knockout (**Fig. 3E**). This may be caused by increased PCNA ubiquitination or decreased total PCNA levels. To measure the relative abundance of total PCNA, we performed tandem mass tag MS using WT, *RAD18*, or *UBE2K* knockout MDA-MB-436 cells with or without USP1 inhibition (Ubiquigent PROTEOME*profiler*, Supplementary Table S5). Proteomics analysis revealed that USP1 inhibition reduced total PCNA protein levels, whereas *RAD18* or *UBE2K* knockout reversed this effect (**Fig. 3F**). Co-treatment with MG132 restored PCNA protein expression, consistent with the rescue of PCNA proteasomal degradation (Supplementary Fig. S3F). *PCNA* mRNA levels remained unchanged at 24 hours after USP1 inhibition, despite decreased PCNA protein levels (Supplementary Fig. S3G). To assess whether total PCNA reduction is required for USP1 inhibitor sensitivity, MDA-MB-436 cells were engineered to express cDNA containing WT or K164R ubiquitin-dead *PCNA* (**Fig. 3G**). Exogenous WT and K164R *PCNA* expression conferred resistance to USP1 but not PARP inhibition (**Fig. 3G**; Supplementary Fig. S3H). These results indicate the aberrant accumulation of mono- and polyubiquitinated PCNA, and consequent PCNA protein degradation, drive *USP1* dependency in *BRCA1/2* mutant tumors.

USP1 and PARP inhibition are synergistic in *BRCA1/2* mutant tumors

To determine whether USP1 and PARP inhibitors synergize in cells, we tested the combination in a panel of *BRCA1/2* WT and mutant cell lines. Cells were assayed in a 9×9 combination matrix, and synergy scores were calculated based on Bliss independence model (38). USP1–PARP inhibitor combination was preferentially synergistic in *BRCA1/2* mutant compared with WT cells (**Fig. 4A**;

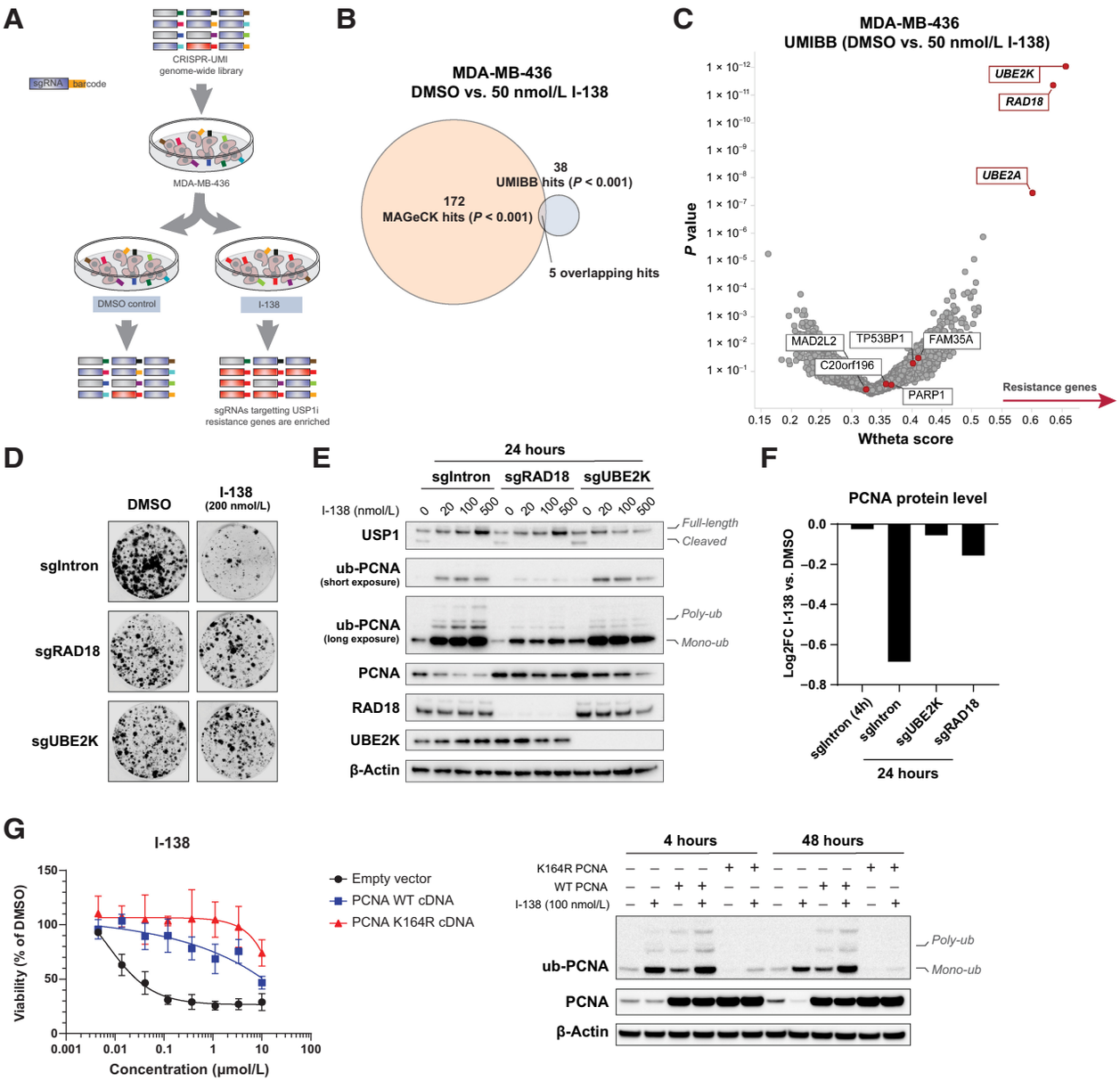

Figure 3.

PCNA ubiquitination and protein loss mediate *USP1* dependency in *BRCA1/2* mutant cells. **A,** CRISPR-Cas9 UMI screen workflow. MDA-MB-436 cells stably expressing *Cas9* were transduced with a genome-wide CRISPR-Cas9 UMI library and cultured for 21 days in the presence of or absence of USP1 inhibitor. **B,** Number of statistically significant hits from MAGeCK and UMIBB analyses ($P < 0.001$) comparing DMSO control and 50 nmol/L treatment groups. **C,** Volcano plot of UMIBB analysis comparing CRISPR-Cas9 UMI screens performed under DMSO control versus 50 nmol/L I-138 conditions in MDA-MB-436 cells. **D,** Isogenic *RAD18* knockout or *UBE2K* knockout cell lines were constructed by transducing targeting sgRNAs into MDA-MB-436 cells stably expressing *Cas9*. Clonogenic assays and (**E**) immunoblotting analyses were performed in these cell lines in the presence or absence of USP1 inhibition. **F,** Quantitation of total PCNA protein levels using tandem mass tag MS (Ubiquigent PROTEOME*profiler*) in WT control, *RAD18* knockout, or *UBE2K* knockout MDA-MB-436 cells following 200 nmol/L I-138 or DMSO mock treatment. Values are represented as log2-fold change from DMSO. **G,** Seven-day CellTiter-Glo assay showing I-138 cell viability dose response (left) and immunoblotting analysis (right) of MDA-MB-436 cells stably expressing empty vector, WT, or K164R ub-dead *PCNA*. Data are presented as mean ± SD, $N = 3$.

Supplementary Fig. S4A). In most *BRCA1/2* mutant cell lines, USP1 inhibition deepened the response to PARP inhibitors (Supplementary Figs. S4A and S4B). Furthermore, combination synergy of USP1–PARP inhibitors was observed using PARP inhibitors with varying PARP1 trapping efficiency (**Fig. 4B**; ref. 39).

To determine whether *BRCA1/2* deficiency is necessary for USP1–PARP inhibitor synergy, we assessed effect of the combination in UWB1.289 isogenic cell lines. The re-expression of *BRCA1* in UWB1.289 abrogated the synergistic effect of USP1 and PARP inhibitors (**Fig. 4C**; Supplementary Fig. S4C). Because PCNA ubiquitination

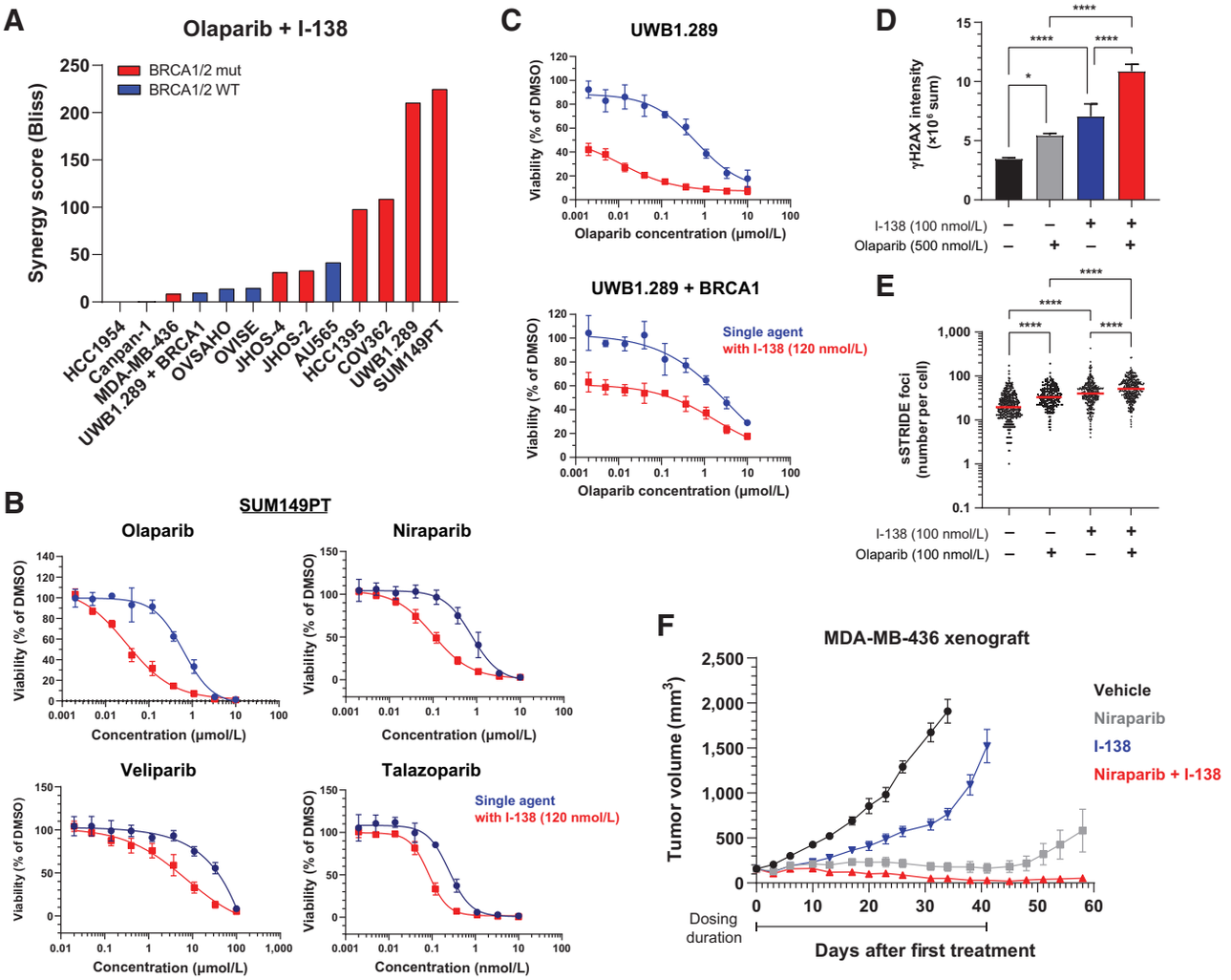

Figure 4.

USP1 and PARP inhibition are synergistic in *BRCA1/2* mutant tumors. **A,** Cell lines were profiled in a 9-point I-138 + olaparib combination dose–response matrix in 384-well plates using a 7-day CellTiter-Glo assay. Synergy score was calculated based on the Bliss model using Combenefit v2.021. **B,** Cell viability dose response of indicated PARP inhibitors in SUM149PT, with and without USP1 inhibitor cotreatment. Cell viability was estimated using 7-day CellTiter-Glo assay, and data are represented as mean ± SD. **C,** Olaparib dose-response in UWB1.289 cells with and without *BRCA1* re-expression, in the presence or absence of 120 nmol/L I-138 co-treatment. Cell viability was estimated using 7-day CellTiter-Glo assay, and data are represented as mean ± SD. **D,** Quantitation of γH2AX intensity in UWB1.289 cells treated with DMSO control or indicated compounds for 72 hours and stained using immunofluorescence. Data are represented as mean ± SD of the total intensity in entire well of a 96-well plate, $N = 3$. Statistical significance was evaluated by ANOVA followed by Dunett *post hoc* test, comparing treatment conditions against DMSO control (****, $P < 0.0001$; *, $P < 0.5$). **E,** Quantitation of single-strand breaks as measured by number of sSTRIDE (intoDNA) foci per cell in UWB1.289 cells treated with indicated compounds for 8 hours. Statistical significance was evaluated by ANOVA followed by Dunett *post hoc* test, comparing treatment conditions against DMSO control (****, $P < 0.0001$). **F,** Tumor volume of MDA-MB-436 xenograft tumors inoculated in NOD SCID mice, treated with vehicle, niraparib (15 mg/kg once daily), I-138 (50 mg/kg once daily), or niraparib + I-138 by oral administration. Drug administration for all groups was stopped on day 41. Data are represented as mean ± SEM, $N = 8$ animals per group.

mediates *USP1* dependency, we evaluated the effect of USP1–PARP inhibitor combination on PCNA posttranslational modifications. Surprisingly, the combination did not further increase PCNA mono- or polyubiquitination compared with USP1 inhibition alone (Supplementary Fig. S4D). To evaluate DNA damage, we measured γH2AX induction in UWB1.289 cells treated with USP1 and PARP inhibitors. Co-treatment with both drugs elicited higher levels of γH2AX compared with either single-agent alone (**Fig. 4D**; Supplementary Fig. S4D). Because PARP1 is recruited to sites of single-strand DNA breaks (SSBs), we reasoned USP1 inhibition-induced DNA damage may amplify PARP inhibitor activity. sSTRIDE Pol1-mediated labeling (40) showed increased SSBs in USP1 inhibitor-treated cells, and additional breaks were detected in cells treated with both USP1 and PARP inhibitors (**Fig. 4E**). Our results suggest USP1 and PARP inhibitors synergize in *BRCA1/2* mutant tumors through increased DNA damage.

Next, we tested the efficacy of USP1–PARP inhibitor combination *in vivo*. I-138 was dosed in mice bearing MDA-MB-436 tumors, either alone or combined with niraparib. USP1 inhibition resulted in modest antitumor activity *in vivo* (**Fig. 4F**). On the other hand, administration

of both drugs resulted in complete tumor regression, and improved efficacy compared with niraparib alone. In summary, these findings demonstrate the combination benefit of USP1 and PARP inhibitors in *BRCA1/2* mutant tumors *in vitro* and *in vivo*.

USP1 dependency extends beyond *BRCA1/2* mutant tumors

DepMap analysis (Public Q122) revealed that in addition to *BRCA1/2* mutant tumors, *USP1* dependency was observed in a subset of *BRCA1/2* WT cancer cell lines enriched in lung and ovarian lineages (**Fig. 5A**). A unifying genetic or histologic feature underlying *USP1* dependency was not identified. *USP1* dependency appears to be selective, because most *BRCA1/2* WT cell lines are not sensitive to USP1 inhibition (**Fig. 5A**; Supplementary Fig. S2B). To explore potential patient expansion, we selected several *USP1* dependent ovarian and lung cancer cell lines for characterization. Interestingly, these cell lines were sensitive to USP1 inhibition but not to olaparib (**Fig. 5B**). To evaluate HR status of these lines, we performed functional RAD51 assays (41). Despite sensitivity to USP1 inhibition, CAOV3, NCI-H1792, and NCI-H1693 cells retained the ability to form RAD51 foci, indicating HR proficiency (**Fig. 5C**).

To elucidate the mechanism of *USP1* dependency, we performed genome-wide CRISPR-Cas9 screening using the lung cancer cell line

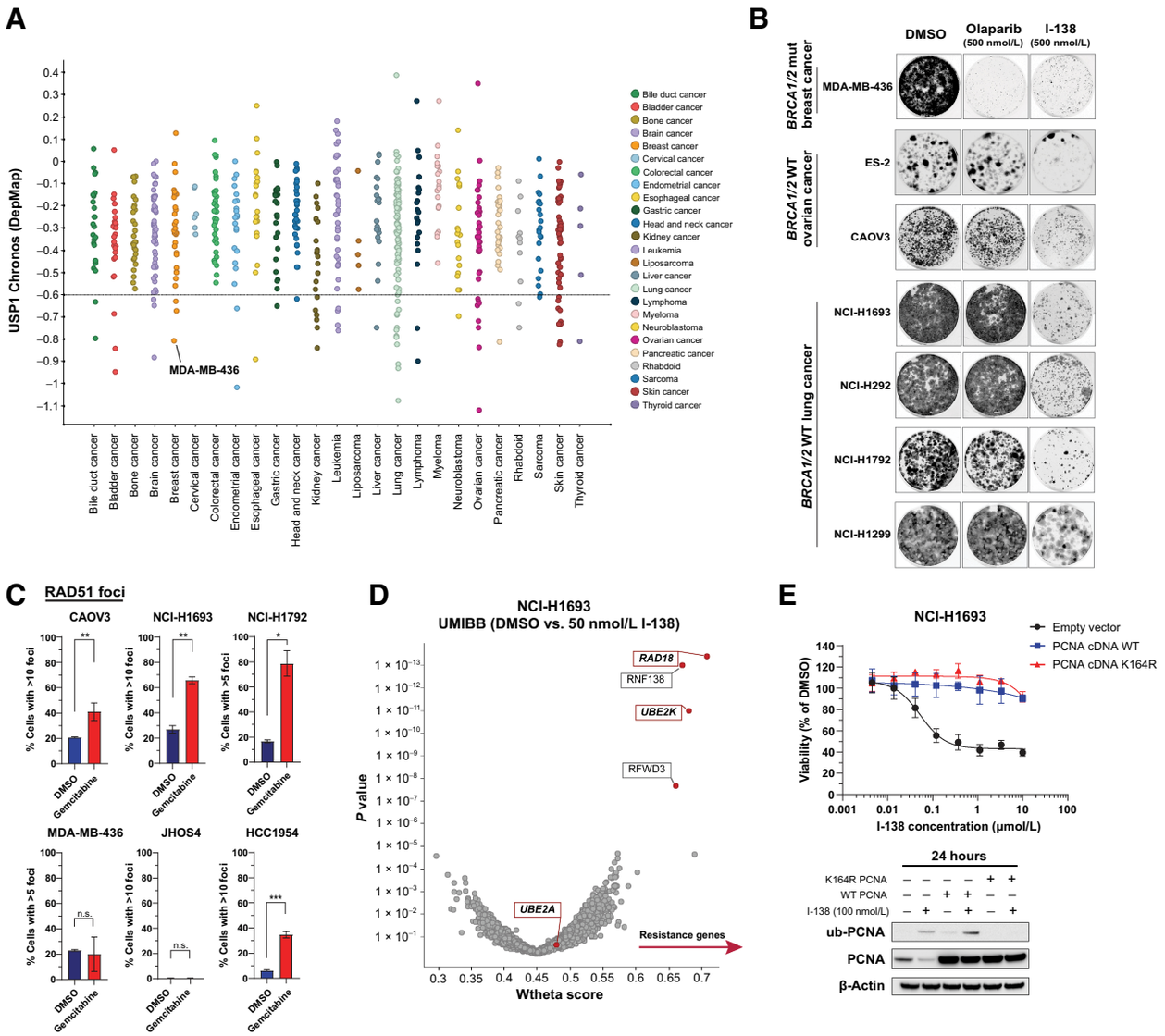

Figure 5.

Ubiquitinated PCNA mediates *USP1* dependency in selected *BRCA1/2* WT cells. **A,** *USP1* dependency estimated using *USP1* Chronos across multiple cancer lineages, extracted from DepMap Public (Q1 2022) CRISPR screening datasets. **B,** Clonogenic assays in cell lines treated with DMSO, olaparib, or I-138 for 10 to 17 days with media change every 3 to 4 days, followed by visualization using crystal violet. **C,** RAD51 foci formation in cell lines treated with DMSO or 100 nmol/L gemcitabine. Data are represented as mean ± SD of averages across three replicate wells. Statistical significance was evaluated using two-tailed Student *t* test (*, $P < 0.05$; **, $P < 0.01$; n.s., not significant). **D,** Volcano plot showing results from UMIBB analysis comparing genome-wide CRISPR-Cas9 UMI screens performed NCI-H1693 cells treated with DMSO or 50 nmol/L I-138. Targeting of genes on the right conferred survival advantage under drug treatment. **E,** I-138 dose–response curves (top) and immunoblotting analysis (bottom) of NCI-H1693 cells stably expressing empty vector, WT *PCNA*, or K164R ubiquitin-dead *PCNA*. Data are represented as mean ± SD.

NCI-H1693 treated with DMSO control, 50 nmol/L (continuous), or 200 nmol/L (5 days on 5 days off) of USP1 inhibitor (**Fig. 3A**). *RAD18* and *UBE2K* were identified as top rescuers, reinforcing the key role of PCNA ubiquitination in *USP1* dependency (**Fig. 5D**; Supplementary Figs. S5A and S5B; Supplementary Tables S6 and S7). Because the same hits were identified in MDA-MB-436, we reasoned that these *BRCA1/2* WT cells may be sensitive to USP1 inhibition following a similar mechanism. We were unable to detect polyubiquitinated PCNA due to limitations of the immunoblot assay, although unmodified PCNA levels were reduced in NCI-H1693 posttreatment (**Fig. 5E**). Importantly, the overexpression of WT or K164R *PCNA* rescued USP1, but not PARP inhibitor sensitivity in NCI-H1693 (**Fig. 5E**; Supplementary Fig. S5C). Our findings suggest that a subset *BRCA1/2* WT cell lines share novel DNA damage vulnerabilities that renders them sensitive to USP1 inhibition due to aberrant PCNA ubiquitination and degradation.

Discussion

In this study, we describe the mechanism of *USP1* dependency in *BRCA1/2* mutant tumors and a subset of *BRCA1/2* WT tumors (**Fig. 6**). USP1 inhibition in sensitive cells results in SSBs, decreased DNA synthesis, reduced replication fork speed, and activation of the ATR–Chk1 signaling cascade. *USP1* dependency is driven by RAD18, an E3 ubiquitin ligase that catalyzes PCNA monoubiquitination, and UBE2K, a novel regulator of PCNA polyubiquitination. We further demonstrate the accumulation of mono- or polyubiquitinated PCNA as a function of USP1 inhibition leads to toxic PCNA protein degradation. USP1–PARP inhibition is synergistic in *BRCA1/2* mutant tumors *in vitro* and *in vivo*. In addition, a subset of HR-proficient *BRCA1/2* WT lung and ovarian cancer cells are sensitive to USP1 inhibition through a similar mechanism. Taken together, these results suggest PCNA-driven *USP1* dependency extends beyond *BRCA1/2* mutant tumors to *BRCA1/2* WT tumors with novel uncharacterized DNA damage vulnerabilities.

USP1 inhibition causes viability loss of *BRCA1/2* mutant but not WT cells, consistent with DepMap and published literature (15). Effect size is a major challenge for synthetic lethal targets, because genetic defects may occur in diverse backgrounds that limit antitumor activity (42, 43). Several *BRCA1/2* mutant cell lines insensitive to USP1 inhibition are also resistant to PARP inhibitors, suggesting similar genetic contexts may drive response to both classes of inhibitors. Presented but unpublished data from us and others have shown USP1 inhibitor activity in *BRCA2* mutant PDX models. Additional preclinical models will help determine USP1 inhibitor activity in broader HR-deficient contexts.

The depletion of *RAD18* or *UBE2K*, in addition to *PCNA* overexpression, rescue USP1 inhibitor sensitivity. Our results indicate PCNA posttranslational modifications and regulation mediate *USP1* dependency. Although RAD18 is known to monoubiquitinate PCNA, we show a novel role for UBE2K in promoting PCNA polyubiquitination and degradation in the context of USP1 inhibition. UBE2K elongates K48-linked chains from monoubiquitinated and K63-linked polyubiquitinated substrates *in vitro* (44, 45). Additional studies are required to understand whether UBE2K directly modifies PCNA. Although MG132 restored PCNA protein levels in USP1 inhibitor-treated cells, we did not observe the expected enrichment of polyubiquitinated PCNA. These suggest that polyubiquitinated PCNA may be degraded through alternative means. In this regard, PCNA polyubiquitination has been shown to promote the recruitment of Spartan protease (46), and a recent study linked Spartan function to USP1 activity on chromatin (14).

In *BRCA1* mutant cells, USP1 inhibition leads to decreased DNA synthesis and accumulation of SSBs. BRCA1 loss-of-function induces ssDNA gap formation during replication (47), which rely on TLS for filling and repair (48, 49). USP1 inhibition may disrupt the ability of *BRCA1* mutant cells to coordinate TLS-mediated ssDNA repair, leading to synthetic lethality. In addition, the accumulation of polyubiquitinated PCNA may divert DNA damage tolerance responses towards TS. Because TS requires BRCA1 (50), USP1 inhibition may lead to inconclusive repair in *BRCA1* mutant cells. Alternatively, *USP1* loss has been shown to promote replication fork reversal, thereby inducing aberrant levels of resection in the context of BRCA1 deficiency (15).

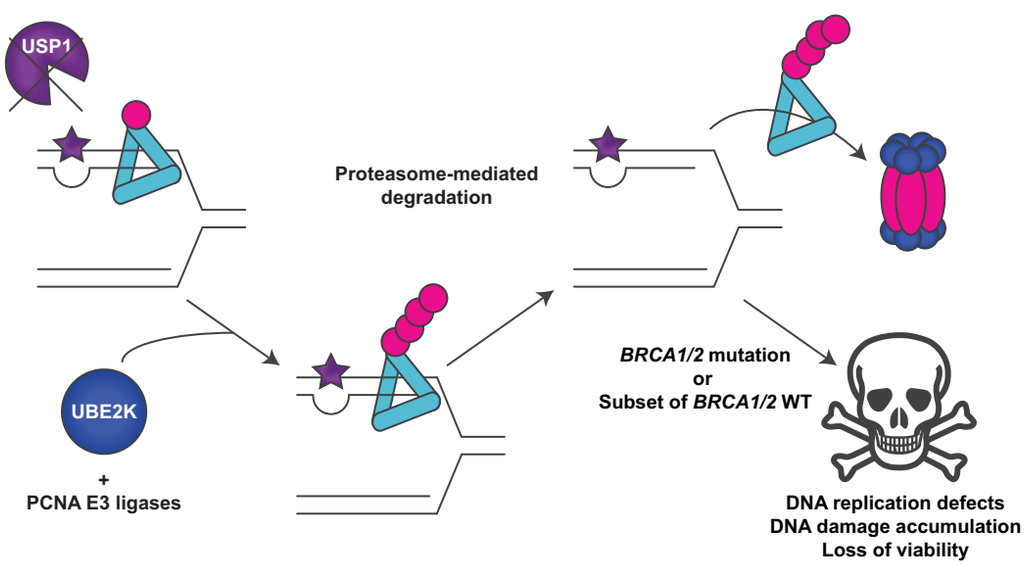

Figure 6.
Mechanism of *USP1* dependency in *BRCA1/2* mutant and selected *BRCA1/2* WT tumors.

CRISPR knockout of genes that mediate PARP inhibitor resistance, such as *TP53BP1*, *REV7*, and *SHLD1–3* (51–53), did not confer USP1 inhibitor resistance. These suggest that resistance to USP1 inhibition may be mechanistically distinct from that of PARP inhibitors. In addition, USP1 inhibition potentiates PARP inhibitor response in *BRCA1/2* mutant tumor models *in vitro* and *in vivo*. The USP1–PARP inhibitor synergy is synthetic lethal with *BRCA1/2* loss of function, as the reconstitution of *BRCA1* eliminated combination benefits. The lack of synergy in *BRCA1/2* WT setting may improve tolerability of the drug combination in patients.

We show a subset *BRCA1/2* WT cell lines to be dependent on *USP1*. In the *BRCA1/2* WT cell-line NCI-H1693, *RAD18* and *UBE2K* knockout rescued USP1 inhibitor sensitivity. Similar to *BRCA1/2* mutant cells, USP1 inhibition reduced unmodified PCNA protein levels, and the overexpression of WT or K164R *PCNA* rescued USP1 inhibitor sensitivity. Our results indicate common characteristics in USP1-dependent cancer cell lines despite their diverse genetic backgrounds. These *BRCA1/2* WT USP1-dependent cell lines are HR proficient, as they retained the ability to form RAD51 foci upon DNA damage. However, these cell lines may harbor other vulnerabilities such as fork protection, TLS, or TS defects (15). Additional work is required to understand the DNA damage vulnerabilities underlying USP1 inhibitor sensitivity in HR-proficient cancers.

Taken together, this study highlights USP1 as a promising target in cancer. In sensitive cells, USP1 inhibition induces aberrant PCNA mono- and polyubiquitination followed by PCNA protein loss. Through this mechanism, USP1 inhibition is efficacious in *BRCA1/2* mutant tumors and a subset of *BRCA1/2* WT tumors with novel uncharacterized DNA damage vulnerabilities. Functional genomics studies suggest the mechanisms of resistance may be nonoverlapping between USP1 and PARP inhibitors. Moreover, the combination of USP1 and PARP inhibitors are highly synergistic in a *BRCA1/2*-dependent fashion. Our results suggest USP1 inhibitors, either alone or in combination, may provide clinical benefits to PARP inhibitor-naïve or resistant patients with potential for indication expansion.

Authors' Disclosures

A. Simoneau reports other support from Tango Therapeutics outside the submitted work. J.L. Engel reports personal fees and other support from Tango Therapeutics outside the submitted work. S.R. Meier reports personal fees and other support from Tango Therapeutics outside the submitted work. A.H. Choi reports personal fees and other support from Equity outside the submitted work. B. Shen reports personal fees from Tango Therapeutics Inc. outside the submitted work. M. Zhang reports personal fees and other support from Tango Therapeutics outside the submitted work. E. Wilker reports other support from Tango Therapeutics outside the submitted work. X. Pan reports other support from Tango Therapeutics outside the submitted work. S. Throner reports a patent for PCT/US2022/016441 pending and a patent for PCT/US2022/020700 pending. Y. Yu reports grants from Tango Therapeutics during the conduct of the study and grants from Tango Therapeutics outside the submitted work. A. Huang reports other support from Tango Therapeutics outside the submitted work. J.N. Andersen reports other support from Tango Therapeutics outside the submitted work. T. Feng reports other support from Tango Therapeutics outside the submitted work and all experiments were paid for by Tango Therapeutics. All authors were employees of Tango Therapeutics at the time this study was performed. No disclosures were reported by the other authors.

Authors' Contributions

A. Simoneau: Conceptualization, data curation, supervision, validation, investigation, visualization, methodology, writing–original draft, writing–review and editing. **J.L. Engel:** Conceptualization, validation, investigation, methodology. **M. Bandi:** Conceptualization, validation, investigation, methodology. **K. Lazarides:** Validation, investigation, methodology. **S. Liu:** Investigation, methodology. **S.R. Meier:** Data curation, software, formal analysis. **A.H. Choi:** Data curation, software, formal analysis, visualization. **H. Zhang:** Investigation, methodology. **B. Shen:** Investigation, methodology. **L. Martires:** Investigation. **D. Gotur:** Investigation, methodology. **T.V. Pham:** Investigation. **F. Li:** Conceptualization, supervision. **L. Gu:** Supervision, methodology, project administration. **S. Gong:** Investigation, methodology. **M. Zhang:** Supervision. **E. Wilker:** Investigation, methodology. **X. Pan:** Supervision, investigation. **D.A. Whittington:** Resources, supervision, project administration. **S. Throner:** Resources. **J.P. Maxwell:** Resources. **Y. Chen:** Supervision, writing–review and editing. **Y. Yu:** Data curation, software, formal analysis, supervision, visualization, methodology. **A. Huang:** Conceptualization, resources, supervision. **J.N. Andersen:** Resources, supervision, writing–review and editing. **T. Feng:** Conceptualization, formal analysis, supervision, investigation, visualization, methodology, writing–original draft, project administration, writing–review and editing.

Acknowledgments

We thank the scientists from ChemPartner, Pharmaron, WuXi AppTec, Biortus, Ubiquigent, and intoDNA for their contributions to this work. We thank Dr. Barbara Weber, Prof. Christopher Lord, and Dr. Natasha Emmanuel for critical reading of the manuscript. We thank Dr. Maria "Masha" Alimova for assistance with high-content imaging analysis.

The publication costs of this article were defrayed in part by the payment of publication fees. Therefore, and solely to indicate this fact, this article is hereby marked "advertisement" in accordance with 18 USC section 1734.

Note

Supplementary data for this article are available at Molecular Cancer Therapeutics Online (http://mct.aacrjournals.org/).

Received June 13, 2022; revised August 8, 2022; accepted October 6, 2022; published first October 12, 2022.

References

1. Lord CJ, Ashworth A. PARP inhibitors: synthetic lethality in the clinic. Science 2017;355:1152–8.
2. Cohn MA, Kowal P, Yang K, Haas W, Huang TT, Gygi SP, et al. A UAF1-containing multisubunit protein complex regulates the Fanconi anemia pathway. Mol Cell 2007;28:786–97.
3. Cohn MA, Kee Y, Haas W, Gygi SP, D'Andrea AD. UAF1 is a subunit of multiple deubiquitinating enzyme complexes. J Biol Chem 2009;284:5343–51.
4. Nijman SMB, Huang TT, Dirac AMG, Brummelkamp TR, Kerkhoven RM, D'Andrea AD, et al. The deubiquitinating enzyme USP1 regulates the Fanconi anemia pathway. Mol Cell 2005;17:331–9.
5. Sims AE, Spiteri E, Sims RJ, Arita AG, Lach FP, Landers T, et al. FANCI is a second monoubiquitinated member of the Fanconi anemia pathway. Nat Struct Mol Biol 2007;14:564–7.
6. Huang TT, Nijman SMB, Mirchandani KD, Galardy PJ, Cohn MA, Haas W, et al. Regulation of monoubiquitinated PCNA by DUB autocleavage. Nat Cell Biol 2006;8:341–7.
7. Hoege C, Pfander B, Moldovan G-L, Pyrowolakis G, Jentsch S. RAD6-dependent DNA repair is linked to modification of PCNA by ubiquitin and SUMO. Nature 2002;419:135–41.
8. Stelter P, Ulrich HD. Control of spontaneous and damage-induced mutagenesis by SUMO and ubiquitin conjugation. Nature 2003;425:188–91.
9. Kannouche PL, Wing J, Lehmann AR. Interaction of human DNA polymerase η with monoubiquitinated PCNA: a possible mechanism for the polymerase switch in response to DNA damage. Mol Cell 2004;14:491–500.
10. Bienko M, Green CM, Crosetto N, Rudolf F, Zapart G, Coull B, et al. Ubiquitin-binding domains in Y-Family polymerases regulate translesion synthesis. Science 2005;310:1821–4.
11. Guo C, Tang T-S, Bienko M, Parker JL, Bielen AB, Sonoda E, et al. Ubiquitin-binding motifs in REV1 protein are required for its role in the tolerance of DNA damage. Mol Cell Biol 2006;26:8892–900.

12. Prakash S, Johnson RE, Prakash L. Eukaryotic translesion synthesis DNA polymerases: specificity of structure and function. Annu Rev Biochem 2005; 74:317–53.
13. Parker JL, Ulrich HD. Mechanistic analysis of PCNA poly-ubiquitylation by the ubiquitin protein ligases Rad18 and Rad5. Embo J 2009;28:3657–66.
14. Coleman KE, Yin Y, Lui SKL, Keegan S, Fenyo D, Smith DJ, et al. USP1-trapping lesions as a source of DNA replication stress and genomic instability. Nat Commun 2022;13:1740.
15. Lim KS, Li H, Roberts EA, Gaudiano EF, Clairmont C, Sambel LA, et al. USP1 is required for replication fork protection in BRCA1-deficient tumors. Mol Cell 2018;72:925–41.
16. Das DS, Das A, Ray A, Song Y, Samur MK, Munshi NC, et al. Blockade of deubiquitylating enzyme USP1 inhibits DNA repair and triggers apoptosis in multiple myeloma cells. Clin Cancer Res 2017;23:4280–9.
17. Ma A, Tang M, Zhang L, Wang B, Yang Z, Liu Y, et al. USP1 inhibition destabilizes KPNA2 and suppresses breast cancer metastasis. Oncogene 2019;38: 2405–19.
18. Williams SA, Maecker HL, French DM, Liu J, Gregg A, Silverstein LB, et al. USP1 deubiquitinates ID proteins to preserve a mesenchymal stem cell program in osteosarcoma. Cell 2011;146:918–30.
19. Liang Q, Dexheimer TS, Zhang P, Rosenthal AS, Villamil MA, You C, et al. A selective USP1–UAF1 inhibitor links deubiquitination to DNA damage responses. Nat Chem Biol 2014;10:298–304.
20. Joseph BA, Stephanos I, Bruce F, Gary G, Minghua W, A CJ, et al. Purinones as ubiquitin-specific protease 1 inhibitors. WO/2017/087837.
21. Veroli GYD, Fornari C, Wang D, Mollard S, Bramhall JL, Richards FM, et al. Combenefit: an interactive platform for the analysis and visualization of drug combinations. Bioinformatics 2016;32:2866–8.
22. Yazinski SA, Comaills V, Buisson R, Genois M-M, Nguyen HD, Ho CK, et al. ATR inhibition disrupts rewired homologous recombination and fork protection pathways in PARP inhibitor-resistant BRCA-deficient cancer cells. Gene Dev 2017;31:318–32.
23. Schindelin J, Arganda-Carreras I, Frise E, Kaynig V, Longair M, Pietzsch T, et al. Fiji: an open-source platform for biological-image analysis. Nat Methods 2012;9: 676–82.
24. Simoneau A, Xiong R, Zou L. The trans cell cycle effects of PARP inhibitors underlie their selectivity toward BRCA1/2-deficient cells. Gene Dev 2021;35: 1271–89.
25. Shields JA, Meier SR, Bandi M, Ferdinez MD, Engel JL, Mulkearns-Hubert EE, et al. VRK1 is a paralog synthetic lethal target in VRK2-methylated glioblastoma. bioRxiv 2022;2021.12.30.474571.
26. Li W, Xu H, Xiao T, Cong L, Love MI, Zhang F, et al. MAGeCK enables robust identification of essential genes from genome-scale CRISPR/Cas9 knockout screens. Genome Biol 2014;15:554.
27. Farmer H, McCabe N, Lord CJ, Tutt ANJ, Johnson DA, Richardson TB, et al. Targeting the DNA repair defect in BRCA mutant cells as a therapeutic strategy. Nature 2005;434:917–21.
28. Bryant HE, Schultz N, Thomas HD, Parker KM, Flower D, Lopez E, et al. Specific killing of BRCA2-deficient tumours with inhibitors of poly(ADP-ribose) polymerase. Nature 2005;434:913–7.
29. Ceccaldi R, Liu JC, Amunugama R, Hajdu I, Primack B, Petalcorin MIR, et al. Homologous-recombination-deficient tumours are dependent on Polθ-mediated repair. Nature 2015;518:258–62.
30. Hewitt G, Borel V, Segura-Bayona S, Takaki T, Ruis P, Bellelli R, et al. Defective ALC1 nucleosome remodeling confers PARPi sensitization and synthetic lethality with HRD. Mol Cell 2021;81:767–83.
31. Kais Z, Rondinelli B, Holmes A, O'Leary C, Kozono D, D'Andrea AD, et al. FANCD2 maintains fork stability in BRCA1/2-deficient tumors and promotes alternative end-joining DNA repair. Cell Rep 2016;15:2488–99.
32. Behan FM, Iorio F, Picco G, Gonçalves E, Beaver CM, Migliardi G, et al. Prioritization of cancer therapeutic targets using CRISPR–Cas9 screens. Nature 6–568:511;2019.
33. Tsherniak A, Vazquez F, Montgomery PG, Weir BA, Kryukov G, Cowley GS, et al. Defining a cancer dependency map. Cell 2017;170:564–76.
34. Rennie M, Arkinson C, Chaugule V, Walden H. Cryo-EM reveals a mechanism of USP1 inhibition through a cryptic binding site. bioRxiv 2022; 2022.04.06.487267.
35. Michlits G, Hubmann M, Wu S-H, Vainorius G, Budusan E, Zhuk S, et al. CRISPR-UMI: single-cell lineage tracing of pooled CRISPR–Cas9 screens. Nat Methods 2017;14:1191–7.
36. Choe KN, Moldovan G-L. Forging ahead through darkness: PCNA, still the principal conductor at the replication fork. Mol Cell 2017;65:380–92.
37. Haldeman MT, Xia G, Kasperek EM, Pickart CM. Structure and function of ubiquitin conjugating enzyme E2–25K: the tail is a core-dependent activity element. Biochemistry-us 1997;36:10526–37.
38. Bliss CI. The toxicity of poisons applied jointly. Ann Appl Biol 1939;26: 585–615.
39. Murai J, Huang SN, Das BB, Renaud A, Zhang Y, Doroshow JH, et al. Trapping of PARP1 and PARP2 by clinical PARP inhibitors. Cancer Res 2012;72:5588–99.
40. Kordon MM, Zarębski M, Solarczyk K, Ma H, Pederson T, Dobrucki JW. STRIDE—a fluorescence method for direct, specific in situ detection of individual single- or double-strand DNA breaks in fixed cells. Nucleic Acids Res 2020;48:e14.
41. Pellegrino B, Herencia-Ropero A, Llop-Guevara A, Pedretti F, Moles-Fernández A, Viaplana C, et al. Preclinical *in vivo* validation of the RAD51 test for identification of homologous recombination-deficient tumors and patient stratification. Cancer Res 2022;82:1646–57.
42. Ashworth A, Lord CJ, Reis-Filho JS. Genetic interactions in cancer progression and treatment. Cell 2011;145:30–8.
43. Ryan CJ, Bajrami I, Lord CJ. Synthetic lethality and cancer: penetrance as the major barrier. Trends Cancer 2018;4:671–83.
44. Christensen DE, Brzovic PS, Klevit RE. E2–BRCA1 RING interactions dictate synthesis of mono- or specific polyubiquitin chain linkages. Nat Struct Mol Biol 2007;14:941–8.
45. Nakasone MA, Majorek KA, Gabrielsen M, Sibbet GJ, Smith BO, Huang DT. Structure of UBE2K–Ub/E3/polyUb reveals mechanisms of K48-linked Ub chain extension. Nat Chem Biol 2022;18:422–31.
46. Centore RC, Yazinski SA, Tse A, Zou L. Spartan/C1orf124, a reader of PCNA ubiquitylation and a regulator of UV-induced DNA damage response. Mol Cell 2012;46:625–35.
47. Cong K, Peng M, Kousholt AN, Lee WTC, Lee S, Nayak S, et al. Replication gaps are a key determinant of PARP inhibitor synthetic lethality with BRCA deficiency. Mol Cell 2021;81:3128–44.
48. Taglialatela A, Leuzzi G, Sannino V, Cuella-Martin R, Huang J-W, Wu-Baer F, et al. REV1-Polζ maintains the viability of homologous recombination-deficient cancer cells through mutagenic repair of PRIMPOL-dependent ssDNA gaps. Mol Cell 2021;81:4008–25.
49. Chen D, Gervai JZ, Póti Á, Németh E, Szeltner Z, Szikriszt B, et al. BRCA1 deficiency specific base substitution mutagenesis is dependent on translesion synthesis and regulated by 53BP1. Nat Commun 2022;13:226.
50. Gervai JZ, Gálicza J, Szeltner Z, Zámborszky J, Szüts D. A genetic study based on PCNA-ubiquitin fusions reveals no requirement for PCNA polyubiquitylation in DNA damage tolerance. DNA Repair (Amst) 2017; 54:46–54.
51. Jaspers JE, Kersbergen A, Boon U, Sol W, DL van, Zander SA, et al. Loss of 53BP1 causes PARP inhibitor resistance in BRCA1-mutated mouse mammary tumors. Cancer Discov 2013;3:68–81.
52. Xu G, Chapman JR, Brandsma I, Yuan J, Mistrik M, Bouwman P, et al. REV7 counteracts DNA double-strand break resection and affects PARP inhibition. Nature 2015;521:541–4.
53. Noordermeer SM, Adam S, Setiaputra D, Barazas M, Pettitt SJ, Ling AK, et al. The Shieldin complex mediates 53BP1-dependent DNA repair. Nature 2018;560: 117–21.